Letter

ADVANCED PHOTONICS

Organic room-temperature phosphorescent polymers for efficient X-ray scintillation and imaging

Juan Wei,[a] Yangyang Jiang,[a] Chenyuan Liu,[a] Jiayu Duan,[a] Shanying Liu,[a] Xiangmei Liu,[a] Shujuan Liu,[a] Yun Ma,[a,*] and Qiang Zhao[a,b,*]

[a]Nanjing University of Posts and Telecommunications, Institute of Advanced Materials and Institute of Flexible Electronics (Future Technology), State Key Laboratory of Organic Electronics and Information Displays and Jiangsu Key Laboratory for Biosensors, Nanjing, China

[b]Nanjing University of Posts and Telecommunications, College of Electronic and Optical Engineering and Microelectronics and College of Flexible Electronics (Future Technology), Jiangsu Province Engineering Research Center for Fabrication and Application of Special Optical Fiber Materials and Devices, Nanjing, China

Abstract. Materials that exhibit visible luminescence upon X-ray irradiation show great potential in the medical and industrial fields. Pure organic materials have recently emerged as promising scintillators for X-ray detection and radiography, due to their diversified design, low cost, and facile preparation. However, recent progress in efficient radioluminescence has mainly focused on small molecules, which are inevitably associated with processability and repeatability issues. Here, a concise strategy is proposed to prepare radioluminescent polymers that exhibit multiple emission colors from blue to yellow with high brightness in an amorphous state by the radical copolymerization of negatively charged polyacrylic acid and different positively charged quaternary phosphonium salts. One of the obtained polymers exhibits excellent photostability under a high X-ray irradiation dosage of 27.35 Gy and has a detection limit of 149 nGy s^{-1}. This performance is superior to that of conventional anthracene-based scintillators. Furthermore, by simply drop-casting a polymer methanol solution on a quartz plate, a transparent scintillator screen was successfully fabricated for X-ray imaging with a resolution of 8.7 line pairs mm^{-1}. The pure organic phosphorescent polymers with a highly efficient radioluminescence were demonstrated for the first time, and the strategy reported herein offers a promising pathway to expand the application range of amorphous organic scintillators.

Keywords: organic scintillator; radioluminescence; room temperature phosphorescence; X-ray imaging; copolymer.

Received Feb. 8, 2022; revised manuscript received Mar. 23, 2022; accepted for publication Apr. 12, 2022; published online May 17, 2022.

[DOI: 10.1117/1.AP.4.3.035002]

1 Introduction

X-ray excited luminescent materials, namely scintillators, have attracted tremendous interest in recent years because they can convert high-energy X-ray photons to low-energy visible luminescence.[1–4] This unique characteristic means that these materials are excellent candidates for various applications in radiation detection,[5–9] medical diagnosis,[10–12] and security inspection.[13–17] However, this intriguing luminescence phenomenon is mainly limited to inorganic materials or heavy metal complexes.[18–22] These inorganic materials have several intrinsic disadvantages, such as harsh preparation conditions, high cost of rare metal resources, and toxicity during biological applications.[23,24] In this context, purely organic materials have been recently developed as promising alternative scintillators due to their low cost, flexibility, and easy preparation process.[25,26] Nevertheless, most known organic scintillators are fluorescent dyes whose luminescence originates from the singlet excited state.[27,28] Previous studies have demonstrated that radioluminescence (RL) is generated by electronic transitions induced by electron impact. Upon X-ray irradiation, the atoms in the organic scintillators interacted

*Address all correspondence to Qiang Zhao, iamqzhao@njupt.edu.cn; Yun Ma, iamyma@njupt.edu.cn

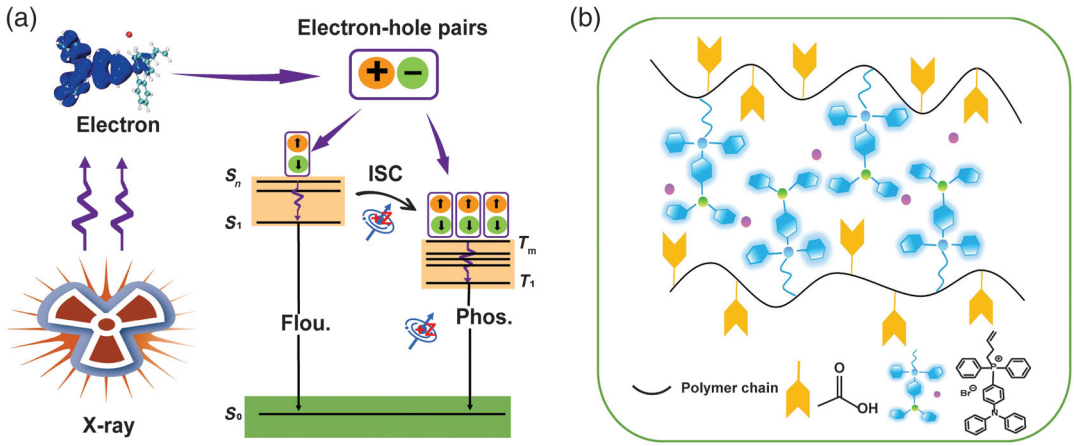

Fig. 1 (a) Schematic illustration of the mechanism of X-ray-irradiated luminescence for organic scintillators. (b) Chemical structures of copolymers P1 to P6.

with high-energy photons by the Compton scattering and photoelectric effect, resulting in the ejection of electrons. Next, the atoms in organic molecules can interact with these electrons to produce secondary electrons and electron–hole pairs. Thus, the RL process of these materials is similar to that of electroluminescence in some respects [Fig. 1(a)].[29,30] Only 25% singlet excitons are used for RL in fluorescent organic scintillators, and the other 75% triplet excitons are wasted due to their dark state characteristics. Therefore, inefficient exciton utilization has obstructed the development of highly efficient organic scintillators.

Thus, the harvesting of triplet excitons in pure organic materials shows promise as an effective strategy for achieving high-performance organic scintillators.[29–32] For example, Huang and coworkers developed a class of organic crystalline materials containing heavy halogen atoms, which can enhance n–π* transitions for facilitating the intersystem crossing (ISC) process. As a result, high-efficiency X-ray-excited luminescence was achieved under ambient conditions due to the utilization of both singlet and triplet excitons.[29] In addition, Yang and coworkers reported a series of thermally activated delayed fluorescence molecules for high-efficiency RL and high-resolution X-ray imaging.[30] Although excellent X-ray scintillation performance has been reported for pure organic small molecule materials, the intrinsic disadvantages of these small molecules in integration and processability for optoelectronic devices hinder their practical application. Compared with organic scintillators based on small molecules, the development of polymeric scintillators may further advance the real-world applications of organic scintillators due to their appealing advantages, including large-area processability, good reproducibility, and high mechanical flexibility.[33–36]

One promising method for achieving high-efficiency pure organic polymer-based scintillators involves the development of room-temperature phosphorescent (RTP) polymeric materials. In this study, a series of RTP polymers were synthesized by the facile radical copolymerization of positively charged quaternary phosphonium salts and negatively charged acrylic acid. Organic quaternary phosphonium derivatives were reported to possess RTP due to their proximity-induced intermolecular electronic coupling in the rigid environment.[37–41] The intense electrostatic interactions between oppositely charged groups and cross-linked hydrogen bonding networks suppressed nonradiative transitions and offered a rigid environment that restricted molecular motions, creating favorable conditions for achieving RTP. Impressively, all the fabricated polymers showed intense RL upon X-ray irradiation. To the best of our knowledge, RL generated from organic RTP polymers upon X-ray irradiation has not yet been reported.

2 Methods

2.1 Scintillator Characterization

The RL spectra were recorded by a QE PRO fiber-coupled fluorescence spectrometer with a Mini-X2 X-ray tube (target material: Au, $P_{max} = 4$ W, $V_{max} = 50$ kV, $I_{max} = 70$ μA, Amptek) as the X-ray source. The X-ray dose rates were altered by adjusting the current of the X-ray tube from 5 to 70 μA. The dose rates under different conditions were calibrated using an X-ray ion chamber dose meter (Radcal Accu-DOSE$^+$, 10X6-60).

2.2 X-ray Imaging

For X-ray imaging, the objects to be measured were placed above the scintillator screens and exposed under a Mini-X2 X-ray tube at an operating voltage of 50 kV and current of 70 μA. Then, the optical path was deflected by a reflector to diminish the negative influence caused by direct X-ray radiation on the camera. The photographs of the polymers under X-ray irradiation were collected by a digital camera (Nikon D850).

2.3 MTF Measurements

Modulation transfer function (MTF) is useful for evaluating the fundamental spatial resolution performance of an imaging system and represents the transfer capability of the input signal modulation of spatial frequency. Here, the MTF was obtained by the slanted-edge method taking an X-ray image of a piece of tungsten (thickness: 1 mm) with sharp edge. The edge spread function (ESF) could be derived from the edge profile of this X-ray image and used to deduce the line spread function (LSF). Finally, the MTF can be defined by the Fourier transform of the LSF as follows:

$$\mathrm{MTF}(\nu) = F(\mathrm{LSF}(\chi)) = F\left(\frac{\mathrm{dESF}(\chi)}{\mathrm{d}\chi}\right),$$

where ν is the spatial frequency and χ is the position of the pixels.

2.4 Scintillator Screen Preparation

P2 (1.0 g) was dissolved in 2 mL CH_3OH; then the quartz plate was treated under UV light for 30 min. The screen was prepared by painting drops of a 300 μL solution.

3 Results

The monomer but-3-en-1-yl(4-(diphenylamino)phenyl)diphenylphosphonium bromide (M1) was prepared by refluxing 4-bromobut-1-ene and 4-(diphenylphosphanyl)-N,N-diphenylaniline in dimethylformamide for 24 h. Then, M1 was copolymerized with acrylic acid at molar ratios of 1/5, 1/10, 1/25, 1/50, 1/100, and 1/200 to prepare a series of copolymers (P1 to P6) [Fig. 1(b)]. ^{1}H, ^{13}C, and ^{31}P nuclear magnetic resonance spectroscopy was used to characterize the monomers, and gel permeation chromatography was used to characterize the polymers (Figs. S1–S9 and Table S1 in the Supplementary Material).

The photoluminescence (PL) properties of polymers P1–P6 were first studied in detail in the solid state. As shown in Fig. 2(a), the prompt PL spectra of all six polymers showed different emission peaks in the range of 464 to 510 nm, displaying similar emission profiles under 400 nm excitation. Impressively, these polymers exhibited a strong luminescence with high quantum efficiencies in the range of 37.69% to 60.27% [Fig. 2(a)]. The delayed PL spectra of these polymers exhibited identical emission profiles but different peaks from 476 to 510 nm (Fig. S10 in the Supplementary Material). Moreover, their emission lifetimes were in the range of 8 to 35.9 ms. The delayed PL intensities and emission decay times of these polymers were significantly enhanced at the low temperature of 77 K (Figs. S11 and S12 in the Supplementary Material), which is indicative of the phosphorescent nature of the delayed emission. It is believed that the enhanced intermolecular interactions and electronic coupling among monomers caused by increasing the proportion of M1 are responsible for the redshift in both fluorescence and RTP.[42]

Next, the photophysical properties of M1 in the poly(methyl methacrylate) (PMMA) films were investigated at 77 K to explore the origins of their RTP. As shown in Fig. S13 in the Supplementary Material, when increasing the M1 content in the PMMA films from 1% to 10% (mass fraction), the PL profiles of the films remained almost constant and no new emission peak appeared. This result indicates that the phosphorescence of the polymers was caused by isolated molecules rather than aggregates. In addition, grazing incidence wide-angle X-ray scattering measurements of P1 to P6 were carried out to study their microstructures. As shown in Fig. S14 in the Supplementary Material, two peaks were obtained. These peaks corresponded to two different luminophore arrangements in the polymers. The low q peak (0.43 Å^{-1}) corresponded to interpolymer chain

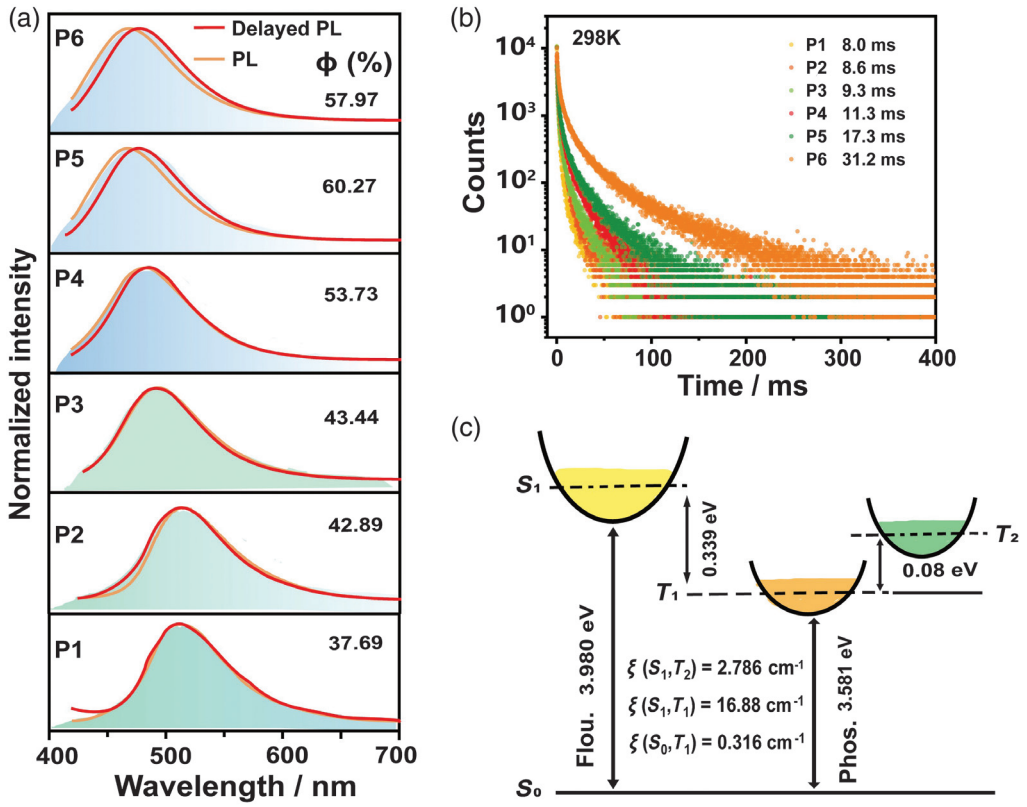

Fig. 2 (a) The PL and delayed PL spectra of polymers P1 to P6 in the solid state at room temperature (excitation at 400 nm). (b) Phosphorescence decay curves of P1 to P6 in the solid state at room temperature (excitation at 400 nm). (c) Calculated energy diagram and spin-orbital coupling (ξ) of M1 monomer.

packing, and the high q peak (1.41 $Å^{-1}$) was assigned to the M1 spacing in one polymer chain. Thus, no π–π interactions were detected among the monomers.[43] To better understand the RTP mechanism, the electronic structure of monomer M1 was studied using time-dependent density functional theory [Fig. 2(c)].[44–49] For M1, the spin-orbit coupling constants (ξ) of S_1 to T_n were calculated to be 16.880 cm^{-1} ($S_1 - T_1$) and 2.786 cm^{-1} ($S_1 - T_2$), indicating an efficient ISC process for the generation of phosphorescence. Overall, it can be concluded that the RTP of these polymers was caused by their monomer molecules.

The X-ray absorption coefficients of M1 and acrylic acid were then recorded. As shown in Fig. 3(a), M1 showed a larger X-ray absorption coefficient than acrylic acid within the energy region of 1 keV to 10 MeV. This indicated that the quaternary phosphonium salts played a crucial role in absorbing X-ray photons, while the acrylic acid group did not play a significant role. The radioluminescent properties of P1 to P6 in the solid state were then investigated. As shown in Fig. 3(c) and Fig. S16 in the Supplementary Material, all six polymers showed obvious RL to the naked eye upon X-ray irradiation, and the RL spectra of these polymers were almost identical to their delayed PL spectra. This result suggests that the triplet excitons of these polymers were fully utilized in the RL generation process. In addition, the amorphous nature of these polymers was confirmed by powder X-ray diffraction patterns (PXRD), as shown in Fig. 3(b).

Among the various copolymerization ratios, the brightest RL was detected when a ratio of 1/10 was used. The RL intensity of the polymers was enhanced with increasing M1 molar ratio from 1/200 to 1/10. However, the RL intensity decreased when the M1 molar ratio was further increased to 1/5 [Fig. 3(d)]. This was potentially because the higher ratio of monomer resulted in a less rigid environment and provided an oxygen shielding effect, resulting in the quenching of triplet excitons. Therefore, P2 (produced with an M1 molar ratio of 1/10) was investigated in detail as a model in the following experiments.

The photostability of scintillators under X-ray irradiation is quite important in practical applications. Thus, the photostability of P2 was determined under a continuous irradiation dosage of 27.35 Gy. As shown in Fig. 3(e), the RL intensity of P2 remained almost unchanged after 20 cycles, indicating its high stability for scintillator applications. In addition, the limit of detection (LOD) is another important parameter for the practical use of scintillators in real-world applications. Figure 3(f) shows that the RL intensities of P2 had a linear dependence on the X-ray dosage. As shown in Fig. 3(f), the LOD of P2 was measured to 149 nGy s^{-1} when the signal-to-noise ratio (SNR) was equal to 3, which is more sensitive than that of anthracene with an LOD of 478 nGy s^{-1}. It is ~37 times lower than the standard dosage of 5.5 μGy s^{-1} found in X-ray biomedical applications.[15] The high photostability and low LOD of P2 mean that it is an ideal candidate for X-ray detection and radiography applications.

To verify the generality of the X-ray excited luminescence of polymeric systems, quaternary phosphonium derivatives of but-3-en-1-yl(9-butyl-9H-carbazol-3-yl)diphenylphosphonium bromide and (6-bromonaphthalen-2-yl)(but-3-en-1-yl)diphenylphosphonium bromide were selected to covalently bond with acrylic acid to prepare RTP polymers. These polymeric

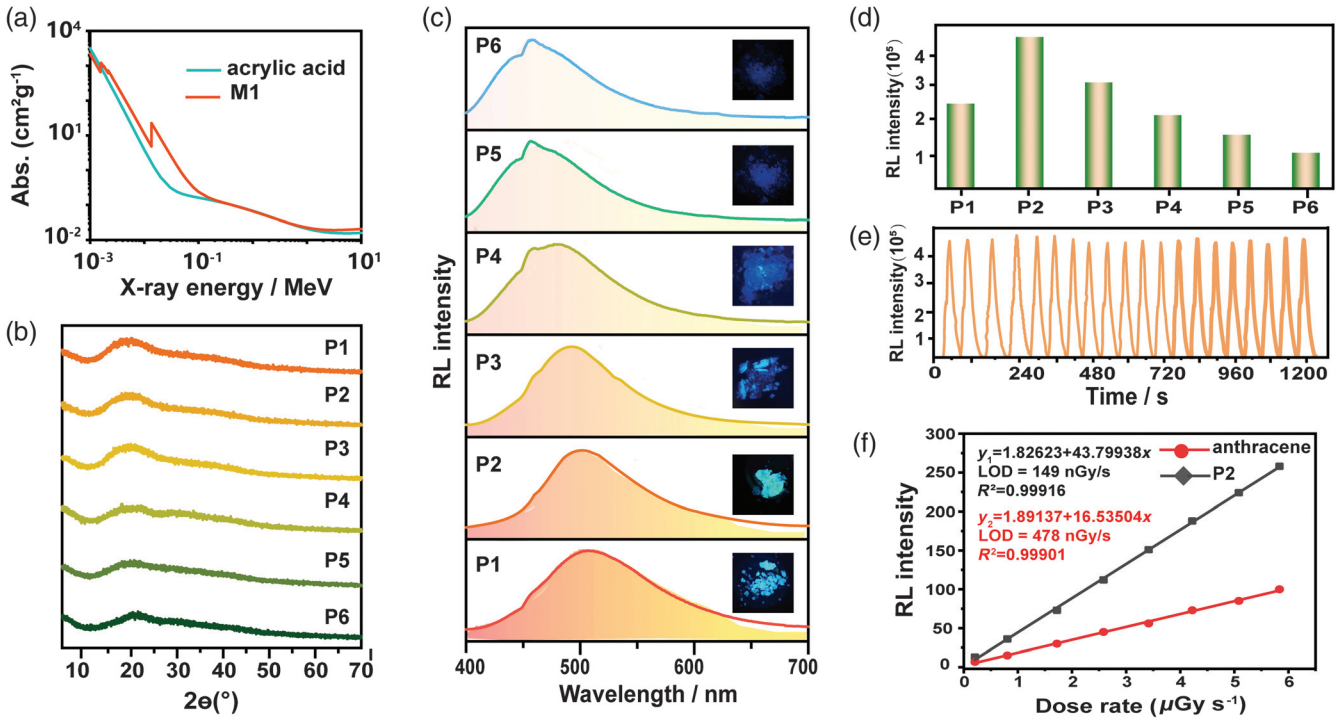

Fig. 3 (a) The X-ray absorption spectra of the M1 and acrylic acid monomers. (b) PXRD patterns of the copolymers P1 to P6. (c) Normalized RL spectra and the related photographs of P1 to P6 under X-ray irradiation. (d) RL intensity changes of P1 to P6 under the same X-ray irradiation condition. (e) The photostability of P2 at 510 nm for continuous X-ray irradiation dosage of 27.35 Gy. (f) LOD (defined as an SNR of 3) and linear behaviors of P2 and anthracene under low-dose-rate X-ray excitation.

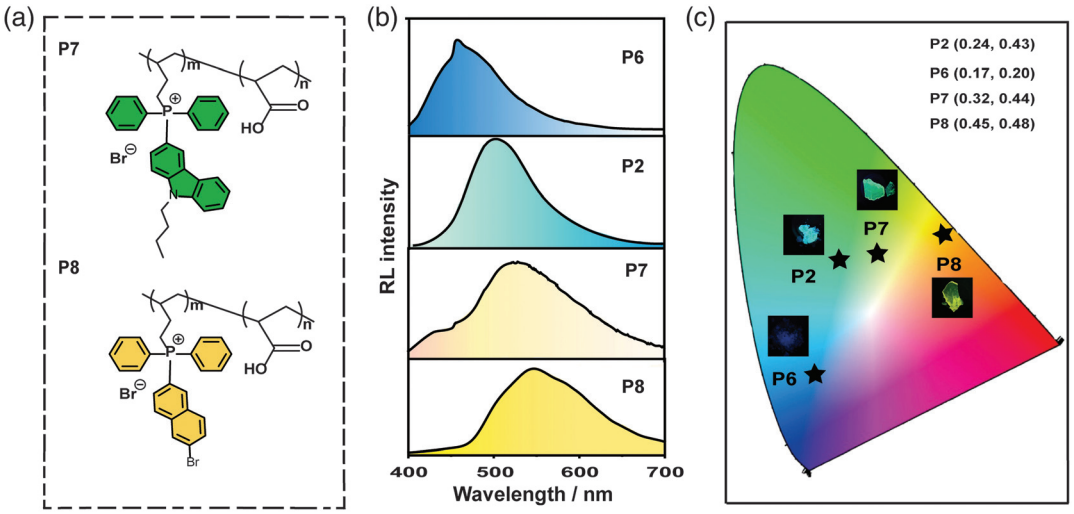

Fig. 4 (a) Chemical structures of P7 and P8. (b) RL spectra of P2, P6, P7, and P8 under X-ray irradiation. (c) CIE chromaticity coordinate diagram of the RL of P2, P6, P7, and P8.

systems were respectively denoted P7 and P8, and they were prepared with a copolymerization ratio of 1/10 [Fig. 4(a)]. As expected, these polymers exhibited RTP under ambient conditions. Furthermore, these two polymers exhibited strong RL under X-ray irradiation [Fig. 4(b), and Figs. S18 and S19 in the Supplementary Material]. Specifically, P7 and P8 displayed maximum RL peaks at 530 and 548 nm, respectively. Also, PXRD patterns confirmed the amorphous nature of P7 and P8 (Fig. S17 in the Supplementary Material). In addition, the X-ray to light conversion efficiencies of P2, P7, and P8, were detected. As shown in Fig. S20 in the Supplementary Material, their values were calculated to be 14,414, 10,584, and 10,436 photons MeV^{-1}, which are comparable to conventional anthracene-based scintillators (15,900 photons MeV^{-1}). The RL wavelength tunability of these polymers is favorable for the construction of a range of X-ray detector arrays with different colors [Fig. 4(c)].

Due to its intense RL, high photostability, and low LOD, P2 was selected for use in an X-ray imaging application (Figs. S20 and S21 in the Supplementary Material). First, transparent

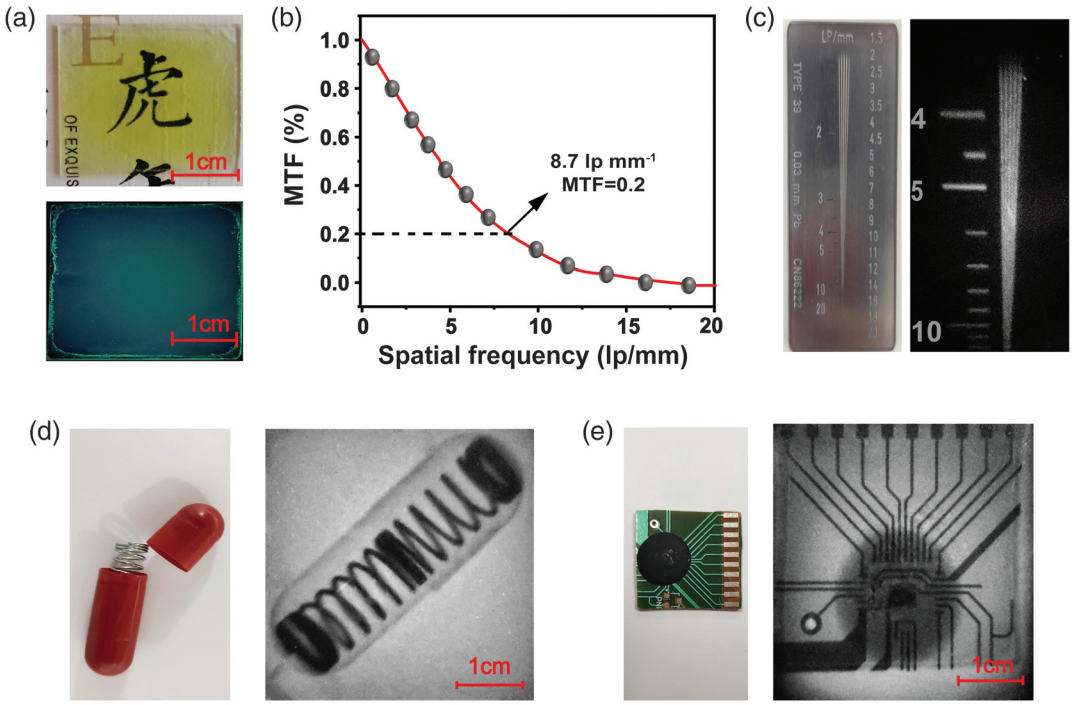

Fig. 5 (a) Photographs of a scintillator screen under daylight and X-ray irradiation. (b) MTF curve of the P2 scintillator screen. (c) Photograph and X-ray image of the standard X-ray test. Bright field and X-ray images of (d) a metallic spring in capsule and (e) a chip card using P2 scintillator screen. X-ray tube voltage, 50 kV; dose rate, 20 mGy s^{-1}; exposure, 15 s.

scintillator screens with different thicknesses (753, 437, and 200 μm) were fabricated by drop-casting of P2 CH_3OH solution (0.5 g/mL) on the quartz plate (Fig. S21 in the Supplementary Material), which was a facile process due to its excellent processability. The prepared screens showed a similar RL color as the solid-state material [Fig. 5(a) and Fig. S21 in the Supplementary Material], and their RL intensities were enhanced with the increase of thin film thickness. Then, X-ray imaging of the scintillator screen through a standard X-ray test pattern plate was performed to measure the maximum possible resolution for radiography using these scintillator screens. The results showed that the scintillator screen with a 437 μm thickness showed the highest maximum resolution among all samples, which suggest that the selected suitable thickness film is quite important. Thus, scintillator screen with a 437 μm thickness was used for X-ray imaging experiments. According to the MTF calculation, a maximum resolution of 8.7 line pairs (lp) mm^{-1} is obtained when MTF value is 0.2 [Fig. 5(c)]. As shown in Fig. 5(b), the line pair notches around 8 lp mm^{-1} were demonstrated, indicating the high-resolution X-ray imaging ability of the P2 screen. As shown in Fig. 5(d), a metal spring was able to be imaged using the prepared scintillator screen even when the spring was in an opaque capsule, suggesting good potential for the inspection of inner structures. Moreover, an electrical chip with metal components inside was used to further demonstrate the X-ray imaging capability of P2 scintillator screen [Fig. 5(e)]. These results demonstrate the excellent potential of organic RTP polymers as scintillator screens for high-quality X-ray imaging.

4 Conclusion

We proposed an effective and general strategy for the preparation of amorphous RTP polymers by incorporating positively charged quaternary phosphonium phosphors into negatively charged polyacrylic acid. It was demonstrated that these polymers can be used as multicolor organic X-ray scintillators with high brightness through the efficient utilization of their triplet excitons. Among the fabricated polymers, P2 was measured to have the brightest RL upon X-ray irradiation, and it also exhibited good photostability after exposure to an X-ray dosage of 27.35 Gy. More importantly, the LOD of P2 was measured to be as low as 149 nGy s^{-1}. Finally, P2 was successfully used to construct a transparent scintillator screen for high-resolution X-ray imaging. Overall, our findings provide a universal design approach for the preparation of amorphous organic materials with a bright RL and offer more possibilities for the use of organic and polymeric amorphous scintillators in optoelectronic and biomedical applications.

Acknowledgments

We gratefully acknowledge the financial support from the National Funds for Distinguished Young Scientists (61825503), the National Natural Science Foundation of China (62075101, 61775101, and 61775103), and the Natural Science Foundation of Jiangsu Province of China (BK20200095). The authors declare no conflict of interest.

References

1. Q. Chen et al., "All-inorganic perovskite nanocrystal scintillators," *Nature* **561**(7721), 88–93 (2018).
2. H. Zhang et al., "Reproducible X-ray imaging with a perovskite nanocrystal scintillator embedded in a transparent amorphous network structure," *Adv. Mater.* **33**(40), 2102529 (2021).
3. Y. M. Yang et al., "X-ray-activated long persistent phosphors featuring strong UVC afterglow emissions," *Light: Sci. Appl.* **7**(1), 88 (2018).
4. J. Perego et al., "Composite fast scintillators based on high-*Z* fluorescent metal–organic framework nanocrystals," *Nat. Photonics* **15**(5), 393–400 (2021).
5. B. G. Durie et al., "High-resolution X-ray luminescence extension imaging," *Science* **190**(4219), 1093–1095 (1975).
6. X. Ou et al., "High-resolution X-ray luminescence extension imaging," *Nature* **590**(7846), 410–415 (2021).
7. W. Zhu et al., "Low-dose real-time X-ray imaging with nontoxic double perovskite scintillators," *Light: Sci. Appl.* **9**(1), 112 (2020).
8. Y. Zou et al., "Nanopolymersomes with an ultrahigh iodine content for high-performance X-ray computed tomography imaging *in vivo*," *Adv. Mater.* **29**(10), 1603997 (2017).
9. Y. He et al., "$CsPbBr_3$ perovskite detectors with 1.4% energy resolution for high-energy γ-rays," *Nat. Photonics* **15**(1), 36–42 (2021).
10. N. Gustavsson et al., "Correlative optical photothermal infrared and X-ray fluorescence for chemical imaging of trace elements and relevant molecular structures directly in neurons," *Light: Sci. Appl.* **10**(1), 151 (2021).
11. P. Pei et al., "X-ray-activated persistent luminescence nanomaterials for NIR-II imaging," *Nat. Nanotechnol.* **16**(9), 1011–1018 (2021).
12. M. Zhang et al., "Metal halide scintillators with fast and self-absorption-free defect-bound excitonic radioluminescence for dynamic X-ray imaging," *Adv. Funct. Mater.* **31**(9), 2007921 (2021).
13. M. Zhuravleva et al., "Praseodymium valence determination in Lu_2SiO_5, Y_2SiO_5 and $Lu_3Al_5O_{12}$ scintillators by X-ray absorption spectroscopy," *Appl. Phys. Lett.* **101**(10), 101902 (2012).
14. Y. X. Zhuang et al., "X-ray-charged bright persistent luminescence in $NaYF_4:Ln^{3+}@NaYF_4$ nanoparticles for multidimensional optical information storage," *Light: Sci. Appl.* **10**(1), 132 (2021).
15. H. Wei et al., "Sensitive X-ray detectors made of methylammonium lead tribromide perovskite single crystals," *Nat. Photonics* **10**(5), 333–339 (2016).
16. M. X. Chen et al., "Organic semiconductor single crystals for X-ray imaging," *Adv. Mater.* **33**(43), 2104749 (2021).
17. X. Chen et al., "X-ray-activated nanosystems for theranostic applications," *Chem. Soc. Rev.* **48**(11), 3073–3101 (2019).
18. H. X. Meng et al., "Highly emissive and stable five-coordinated manganese (II) complex for X-ray imaging," *Laser Photonics Rev.* **15**(11), 2100309 (2021).
19. X. Wang et al., "Perovskite-nanosheet sensitizer for highly efficient organic X-ray imaging scintillator," *ACS Energy Lett.* **7**(1), 10–16 (2022).
20. L. L. Wang et al., "Ultra-stable $CsPbBr_3$ perovskite nanosheets for X-ray imaging screen," *Nano-Micro Lett.* **11**(1), 52 (2019).
21. S. Cho et al., "Hybridisation of perovskite nanocrystals with organic molecules for highly efficient liquid scintillators," *Light: Sci. Appl.* **9**(1), 156 (2020).
22. J. X. Wang et al., "Nearly 100% energy transfer at the interface of metal-organic frameworks for X-ray imaging scintillators," *Matter* **5**(1), 253 (2022).
23. M. Baroncini et al., "Rigidification or interaction-induced phosphorescence of organic molecules," *Chem. Commun.* **53**(13), 2081 (2017).
24. S. Hirata et al., "Efficient persistent room temperature phosphorescence in organic amorphous materials under ambient conditions," *Adv. Funct. Mater.* **23**(27), 3386–3397 (2013).
25. Z. Y. Yang et al., "Intermolecular electronic coupling of organic units for efficient persistent room-temperature phosphorescence," *Angew. Chem. Int. Ed.* **55**(6), 2181–2185 (2016).

26. O. Bolton et al., "Activating efficient phosphorescence from purely organic materials by crystal design," *Nat. Chem.* **3**(3), 205–210 (2011).
27. J. B. Birks, "Semi-empirical calculation of quenching factor for scintillators: new results," *Proc. Phys. Soc.* **64**(10), 874 (1951).
28. B. Fraboni et al., "Radiation detectors: ionizing radiation detectors based on solution-grown organic single crystals," *Adv. Funct. Mater.* **26**(14), 2276–2291 (2016).
29. X. Wang et al., "Organic phosphors with bright triplet excitons for efficient X-ray-excited luminescence," *Nat. Photonics* **15**(3), 187–192 (2021).
30. W. B. Ma et al., "Thermally activated delayed fluorescence (TADF) organic molecules for efficient X-ray scintillation and imaging," *Nat. Mater.* **21**(2), 210–216 (2021).
31. S. Garain et al., "Arylene diimide phosphors: aggregation modulated twin room temperature phosphorescence from pyromellitic diimides," *Angew. Chem. Int. Ed.* **133**(22), 12431–12435 (2021).
32. X. Ma et al., "Amorphous pure organic polymers for heavy-atom-free efficient room-temperature phosphorescence emission," *Angew. Chem. Int. Ed.* **57**(34), 10854–10858 (2018).
33. X. Y. Dou et al., "Color-tunable excitation-dependent, and time-dependent afterglows from pure organic amorphous polymers," *Adv. Mater.* **32**(47), 2004768 (2020).
34. N. Gan et al., "Recent advances in polymer-based metal-free room-temperature phosphorescent materials," *Adv. Funct. Mater.* **28**(51), 1802657 (2018).
35. M. M. Fang et al., "Recent advances in purely organic room temperature phosphorescence polymer," *J. Polym. Sci.* **37**(4), 383–393 (2019).
36. T. Zhang et al., "Molecular engineering for metal-free amorphous materials with room-temperature phosphorescence," *Angew. Chem., Int. Ed.* **59**(28), 11206 (2020).
37. P. Alam et al., "Two are better than one: a design principle for ultralong-persistent luminescence of pure organics," *Adv. Mater.* **32**(22), 2001026 (2020).
38. G. Chen et al., "Anion-regulated transient and persistent phosphorescence and size-dependent ultralong afterglow of organic ionic crystals," *J. Mater. Chem. C* **7**(46), 14535–14542 (2019).
39. G. Chen et al., "Photophysical tuning of organic ionic crystals from ultralong afterglow to highly efficient phosphorescence by variation of halides," *J. Phys. Chem. Lett.* **9**(21), 6305–6311 (2018).
40. P. F. She et al., "Lifetime-tunable organic persistent room-temperature phosphorescent salts for large-area security printing," *Sci. China Mater.* **64**(6), 1485–1494 (2021).
41. P. F. She et al., "Controllable photoactivated organic persistent room-temperature phosphorescence for information encryption and visual temperature detection," *Cell Rep. Phys. Sci.* **2**(7), 100505 (2021).
42. J. Yuan et al., "Activating intersystem crossing and aggregation coupling by CN-substitution for efficient organic ultralong room temperature phosphorescence," *J. Phys. Chem. C* **124**, 18, 10129–10134 (2020).
43. S. Kee et al., "Controlling molecular ordering in aqueous conducting polymers using ionic liquids," *Adv. Mater.* **28**(39), 8625–8631 (2016).
44. S. Grimme et al., "Effect of the damping function in dispersion corrected density functional theory," *J. Comput. Chem.* **32**(7), 1456–1465 (2011).
45. S. Grimme et al., "A consistent and accurate *ab initio* parametrization of density functional dispersion correction (DFT-D) for the 94 elements H-Pu," *J. Chem. Phys.* **132**(15), 154104 (2010).
46. F. Neese, "The ORCA program system," *WIREs Comput. Mol. Sci.* **2**(1), 73–78 (2012).
47. F. Neese, "Software update: the ORCA program system, version 4.0," *WIREs Comput. Mol. Sci.* **8**(1), e1327 (2018).
48. T. Lu et al., "A multifunctional wavefunction analyzer," *J. Comput. Chem.* **33**(5), 580–592 (2012).
49. W. Humphrey et al., "VMD: visual molecular dynamics," *J. Mol. Graphics* **14**(1), 33–38 (1996).

Juan Wei is a PhD student at Nanjing University of Posts and Telecommunications under the supervision of Prof. Qiang Zhao. Her research focuses on the development of organic room-temperature phosphorescent polymers for various advanced photonic applications.

Yun Ma received his master's degree from Nanjing University of Posts and Telecommunications in 2012, under the supervision of Prof. Qiang Zhao and his PhD from Hong Kong Baptist University in 2015, under the supervision of Prof. Wai Yeung Wong. He is currently a full-time professor at Nanjing University of Posts and Telecommunications. His research focuses on the development of stimuli-responsive materials for various optoelectronic devices.

Qiang Zhao received his PhD from Fudan University in 2007. He then became a postdoctoral fellow at Nagoya University of Japan. He joined Nanjing University of Posts and Telecommunications in 2008. He was promoted as a full professor in 2010. His research area is organic optoelectronics, including the design, synthesis and excited-state tuning of organic semiconductors for applications in optoelectronic devices and biomedical fields.

Biographies of the other authors are not available.